

Accurate Planar Tracking With Robust Re-Detection

Jonas Serych Jiri Matas

Visual Recognition Group, Faculty of Electrical Engineering, Czech Technical University in Prague

{serycjon, matas}@fel.cvut.cz

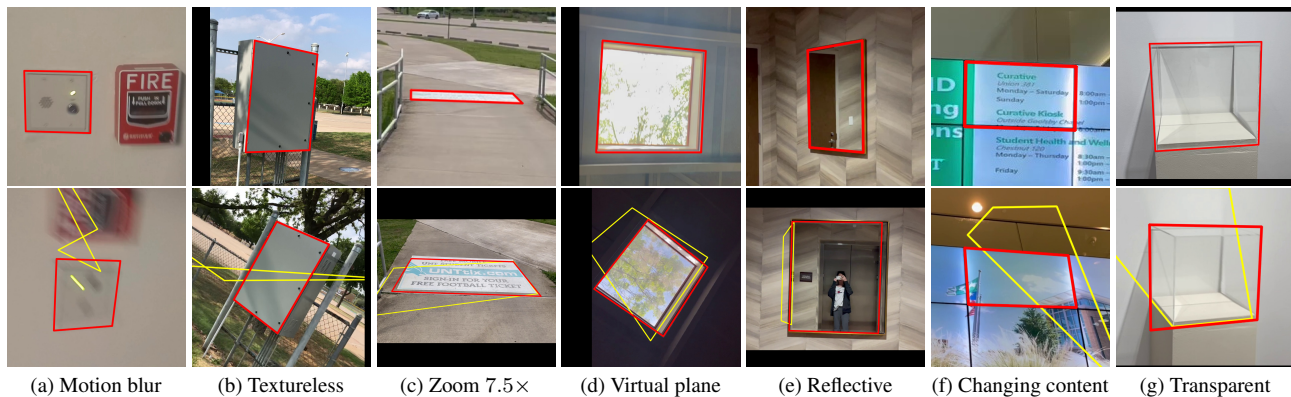


Figure 1. Challenging scenarios from PlanarTrack [16]. Top: the initial frame, the tracked region in red. Bottom: the proposed **WOFTSAM** output in red, the best performing tracker on the dataset in prior art [16] WOFT [23] in yellow. WOFTSAM out-performs the prior state-of-the-art by introducing a segmentation-based robust re-detection mechanism. Examples include planar tracking challenges like perspective distortion, rotation, and scale change (a)-(c) as well as unconventional targets that change appearance in the video (d)-(g). The last column depicts a partial failure.

Abstract

We present *SAM-H* and *WOFTSAM*, novel planar trackers that combine robust long-term segmentation tracking provided by SAM 2 [22] with 8 degrees-of-freedom homography pose estimation. *SAM-H* estimates homographies from segmentation mask contours and is thus highly robust to target appearance changes. *WOFTSAM* significantly improves the current state-of-the-art planar tracker WOFT [23] by exploiting lost target re-detection provided by *SAM-H*. The proposed methods are evaluated on POT-210 [14] and PlanarTrack [16] tracking benchmarks, setting the new state-of-the-art performance on both. On the latter, they outperform the second best by a large margin, +12.4 and +15.2 pp on the $p@15$ metric. We also present improved ground-truth annotations of initial PlanarTrack poses, enabling more accurate benchmarking in the high-precision $p@5$ metric. The code and the re-annotations are available at <https://github.com/serycjon/WOFTSAM>.

1. Introduction

Planar object tracking — the task of localizing and estimating the pose of a flat object in video frames — is a computer vision problem with many applications in augmented reality,

robotics, and 3D reconstruction. The pose of a planar object is fully described by a 8 degrees-of-freedom homography transformation [10], which has traditionally been estimated using keypoint detection and matching (e.g. SIFT [18]), followed by robust model fitting via RANSAC [9]. Despite the long history of homography estimation [4, 18, 19, 23, 26, 28], planar tracking in general conditions is far from solved. Challenges include strong perspective distortion, textureless surfaces, rotation, motion blur, highly reflective surfaces, transparent and virtual targets, and surfaces with dynamically changing appearance as illustrated in Fig. 1.

The current state-of-the-art approach to this task is WOFT [23], which estimates homography pose from deep optical flow correspondences [24]. WOFT (together with [28]) achieved top performance on several benchmarks, including POT [14, 15], POIC [7], and PlanarTrack [16]. While WOFT performs reliably on well-textured objects and in short-term tracking scenarios, it struggles to recover once the target is lost — due to occlusions, out-of-view motion, or strong motion blur — because it lacks a robust mechanism for re-detection.

Recent advances in general object tracking, such as SAM 2 [22], have demonstrated strong long-term tracking performance via robust and high-quality segmentation. However,

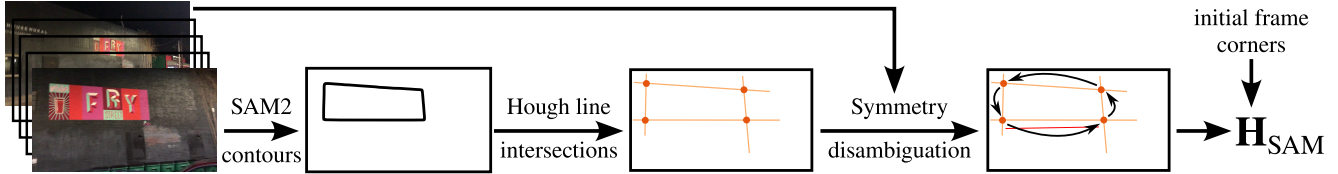


Figure 2. Overview of the SAM-H procedure for estimating homography from a segmentation tracker output. First, corners of the SAM 2 [22] mask are robustly extracted via intersection of Hough lines. Next, a symmetry disambiguation process based on a motion model and the target appearance decides which corner is which and a SAM-H homography is estimated. The SAM-H homography pose provides an initialization for target re-detection ability of the proposed WOFTSAM planar tracker.

segmentation trackers do not provide precise geometric pose and segmentation alone yields only a rough object location.

In the paper, we propose a novel method that integrates a segmentation-based tracker with robust analysis of region boundaries and optical-flow-based homography estimation to track planar objects under challenging conditions. The approach integrates the long-term resilience of segmentation with the fine-grained precision of optical flow and homography estimation.

The contributions of the paper are: (i) SAM-H: a method for long-term homography tracking based on a general segmentation tracker, (ii) WOFTSAM: a planar tracker that significantly improves the current state-of-the-art WOFT [23] by integrating robust target re-detection capability of SAM-H, achieving state-of-the-art on POT-210 [14] and PlanarTrack [16], (iii) precise re-annotation of initial frame ground truth in the PlanarTrack [16] benchmark, improving the PlanarTrack suitability for evaluation of high-precision methods. The effects of the initial frame ground-truth accuracy are significant, see Table 3.

2. Related Work

Planar object tracking via homography estimation is a classical computer vision problem. Early approaches align an image template to each video frame using intensity-based registration, *e.g.* Lucas–Kanade [1, 19]. Efficient Second-order Minimization (ESM) [3] and its extensions [5–7] accelerate and improve robustness of Lucas–Kanade by using second-order approximations and feature pyramids. However, direct alignment methods typically struggle under large blur, occlusion or out-of-view conditions common in real-world planar tracking.

A more robust class of trackers uses feature matching: detect and describe keypoints on the object and match them to each frame. Standard pipelines use SIFT [18], SURF [2] or other classical features and estimate a homography by RANSAC [9]. Modern variants replace hand-crafted descriptors with learned ones (*e.g.* GIFT [17], or LISRD [21]). Instead of matching keypoints independently, Gracker [26] and CGN [13] formulate the task as a graph matching problem. The keypoint-based methods handle occlusion and

viewpoint change better, but require rich texture.

Another class of methods is based on deep learning. In HDN [27], the homography is estimated by regressing positions of four control points after a rough alignment via an estimated similarity transform. The HVC-Net [28] also regresses the four control points and on top of that models uncertainty and occlusions. In contrast, WOFT [23] estimates the homography from dense optical flow correspondences and regressed per-correspondence reliability weights. WOFT also pre-warps the optical flow estimation image inputs so that there is only a relatively small residual flow, which is the scenario that optical flow methods are trained for.

Outside of planar tracking, the broader general object tracking field has recently shifted toward segmentation-based methods. Models like SAM 2 [22] or DAM4SAM [25] achieve robust long-term tracking with precise segmentation masks, but they do not explicitly model the underlying geometry and do not provide homographies. We propose to utilize the long-term stable segmentation masks for homography estimation.

3. Method

Given a video sequence $(I_t)_{t=0}^T$ and a target X_0 on the first frame, the goal is to estimate a homography matrix $\mathbf{H}_t \in \mathbb{R}^{3 \times 3}$ in each frame I_t , such that warping the target with the estimated homography gives the target pose $X_t = \mathcal{W}(\mathbf{H}_t, X_0)$ in the current frame. The target is usually specified by four control points $X_0 = (x_0, x_1, x_2, x_3)$, $x_i \in \mathbb{R}^2$, forming a quadrilateral.

The overall idea of our approach is to add robust re-detection ability to the state-of-the-art WOFT [23] method (overview in Figure 3). WOFT consists of two main steps. First, the initial I_0 and the current frame I_t are aligned to a similar view via some initial homography estimate (a previous frame pose) *pre-warp*, then a refined residual homography is estimated from *optical flow* correspondences.

The optical flow based homography estimation is precise, but relies heavily on a good pre-warp. The previous frame pose used for pre-warping in WOFT works well in short-term tracking, but is not capable of robust re-detection after occlusions or multi-frame tracking failures caused by *e.g.*

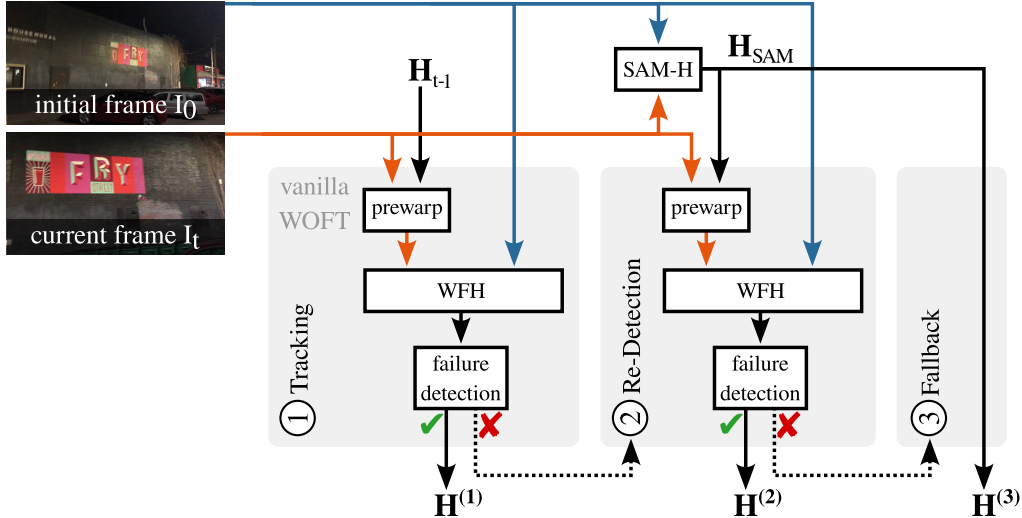


Figure 3. Overview of the proposed WOFTSAM planar tracker. Like in WOFT [23], tracking ① consists of image pre-warping with the previous frame homography \mathbf{H}_{t-1} and homography estimation via the Weighted Flow Homography (WFH) [23] module. If the homography estimation fails (detected by correspondence support set being small), WOFTSAM does a re-detection step ②, in which the SAM-H output \mathbf{H}_{SAM} acts as the pre-warping homography. If even the re-detection fails, WOFTSAM falls back ③ to \mathbf{H}_{SAM} .

motion blur. Instead, we propose to use a pre-warp homography estimated from a segmentation mask S_t provided by a robust long-term segmentation tracker.

Many real life planar objects and nearly all the targets in planar tracking benchmarks [7, 14–16] have quadrilateral shape, meaning that the four homography control points X_0 defining the target align with real corners of the tracked object and the target segmentation is the quadrilateral (up to occlusions and out-of-view). We rely on this fact in the proposed segmentation-tracking-based homography re-detection module SAM-H (see Fig. 2 for an overview).

SAM-H: from segmentation mask to homography. In particular, we prompt the SAM 2 [22] segmentation tracker with a quadrilateral mask specified by the initial coordinates X_0 and let it track, providing a segmentation mask S_t on each frame. Next, we fit four lines to the contours of S_t via Hough transform [8, 11] and find their intersections \tilde{X}_t , keeping only the ones close to the mask and discarding the extra intersections.

The resulting points cannot be used directly to estimate the homography, since the quadrilateral is invariant to cyclical shifts of the corners due to its symmetrical shape. The goal of the *symmetry disambiguation* step is to order the detected Hough lines intersections \tilde{X}_t to form X_t which matches to the initial corners X_0 . In the standard tracking regime, we choose the cyclical shift that minimizes the distance between X_{t-1} and X_t (zero velocity motion model).

In the re-detection regime, where the target is re-detected after being lost due to occlusions, out-of-view, or tracking failure, we do not rely on previous poses and instead the al-

gorithm analyzes the appearance of the target to find the best cyclical corner shift. In particular, we compare DINOv2 [20] features extracted from the current frame object crop with features extracted from a template view warped to the four cyclically shifted candidate views. A target is declared re-detected, if the same cyclical shift (0-shift is based on the zero velocity motion model) has the best DINOv2 feature similarity for $\theta_r = 5$ consecutive frames. This prevents noisy re-detections on the difficult frames when the object may not be well visible yet. The DINOv2 features are robust to wide range of appearance changes and to imprecise alignment, making them suitable for the task.

After the symmetry disambiguation, a homography is estimated from the shifted corners. In case all four points are visible and detected, we directly compute the homography \mathbf{H}_t between the X_0 and X_t . In case less than four points are detected, the homography \mathbf{H}_t is composed of the homography to the previous frame \mathbf{H}_{t-1} and a residual transformation $\Delta\mathbf{H}_{t-1 \rightarrow t}$. When at least two points are visible, $\Delta\mathbf{H}$ is a 4-DoF similarity transform (translation + rotation + single scale) estimated from the motion of the visible points since the previous frame. When only a single point is visible, $\Delta\mathbf{H}$ is a pure 2-DoF translation of the visible point with respect to the previous frame. We call this method **SAM-H**.

WOFTSAM: precise tracking with robust re-detection. While the SAM-H homographies \mathbf{H}_{SAM} are not pixel- or sub-pixel-perfect, they serve as a robust re-initialization for the proposed WOFTSAM planar tracker. In particular, the WOFTSAM does up to two attempts to estimate the homography in the current frame with the weighted opti-

Segmentation tracker	p@5 \uparrow	p@15 \uparrow
SAM 2 [22]	59.6	77.2
DAM4SAM [25]	58.6	77.7
SAM2 ⁺	62.0	80.0

Table 1. Ablation — the choice of the segmentation module for the SAM-H homography estimation, evaluated on PlanarTrack_{TST} [16]. All further results use our SAM2⁺ configuration, which performed the best. SAM2⁺ is the original SAM 2 [22], changed to use memory temporal stride 5 and disabling memory updates when the object is not visible. These are two simple and yet highly effective modifications introduced by DAM4SAM. The p@5 and p@15 metrics are explained in Sec. 4.

cal flow homography estimation module (WFH) from [23]. First, the current frame I_t is pre-warped ($\mathcal{W}(\cdot, \cdot)$) with the previous frame pose \mathbf{H}_{t-1} followed by the WFH homography estimation $\mathbf{H}^{(1)} = \text{WFH}(I_0, \mathcal{W}(\mathbf{H}_{t-1}, I_t))$. If the first attempt fails, as judged by the support set size of the homography (less than 20% of inliers as in [23], see Section D in the supplementary for an ablation), a re-detection attempt is made. The current frame I_t is pre-warped with the segmentation-based \mathbf{H}_{SAM} to get $\mathbf{H}^{(2)} = \text{WFH}(I_0, \mathcal{W}(\mathbf{H}_{\text{SAM}}, I_t))$. When even this second attempt fails the support set size check, the \mathbf{H}_{SAM} is returned as the best-guess output.

3.1. Implementation details

For the segmentation tracker we use the SAM2.1.hieratiny variant in default configuration, except for two improvements from DAM4SAM [25] — we set the memory temporal stride to 5, and disable memory updates when the target is not present. We found this to perform better than both plain SAM 2 [22] and the full DAM4SAM [25]. See Tab. 1 for details. For optical flow homography estimation we use the pre-trained version of RAFT [24] from [23].

For the symmetry disambiguation, we use a template view either from the initial frame I_0 , or from a later one where the target appears biggest-so-far, but before any of the four corners becomes lost, *i.e.*, before any re-detections. This helps in cases when the target has low resolution (far away or zoomed out) on the first frame. We scale the cropped target views to a standard 224×224 resolution and use the dinov2_vits14_reg model [20] features (16×16 featuremap resolution, 384 channels). Each featuremap vector is L2-normalized and the similarity is computed as a dot-product between the warped template view and the current view features. WOFTSAM runs at 2.4 FPS on an NVIDIA RTX A5000 GPU. Details in Section E in supplementary. For details of the Hough transform line search, see Section F in supplementary.

method	POT-210 [14]		PT _{TST} [16]	
	p@5	p@15	p@5	p@15
SIFT [14, 18]	65.8	69.6	17.6	26.7
LISRD [14, 21]	68.3	79.2	22.0	37.2
HDN [27]	70.9	92.4	26.6	56.5
CGN [13]	78.5	93.3	–	–
HVC-Net [28]	<u>91.4</u>	<u>95.8</u>	42.0	63.1
WOFT [23]	90.0	95.4	43.6	64.8
WOFTSAM	91.9	97.5	<u>51.5</u>	<u>77.2</u>
SAM-H	64.4	89.0	62.0	80.0

Table 2. Precision on the POT-210 [14] benchmark with improved ground-truth from [23] and on PlanarTrack_{TST} [16] (PT_{TST}). Higher is better. The proposed WOFTSAM tracker achieves new state-of-the-art on both datasets. In both cases, the segmentation based robust re-detection improves over the baseline WOFT. The improvement is particularly large on the more difficult PlanarTrack dataset. The proposed SAM-H module alone, although not very accurate (POT-210 results), achieves the best results on PlanarTrack because of its ability to track some of the highly unconventional targets present in part of the benchmark. Explained in detail in Sec. 4.2.

4. Experiments

We evaluate the proposed methods on two recent planar tracking benchmarks, POT-210 [14] and PlanarTrack [16]. The POT-210 benchmark contains videos of 30 objects. There are 6 videos for each target, each focusing on one challenging attribute — scale change, rotation, perspective distortion, motion blur, occlusions, target out-of-view — plus one unconstrained video combining all the above.

The recent PlanarTrack benchmark with 300 test videos is similar to the POT unconstrained category, but more challenging as shown in [16], with extreme scale changes, distractors, reflections, transparent objects and other challenges.

In both benchmarks, the evaluation is based on the *alignment error*,

$$e_{\text{AL}}(\mathbf{H}; \mathbf{H}^*, X) = \sqrt{\frac{1}{4} \sum_{i=1}^4 (\mathcal{W}(\mathbf{H}^*, \mathbf{x}_i) - \mathcal{W}(\mathbf{H}, \mathbf{x}_i))^2}, \quad (1)$$

comparing the positions of four template control points, $X = \{x_1, x_2, x_3, x_4\}$ warped ($\mathcal{W}(\cdot, \cdot)$) to the current frame by the ground truth homography \mathbf{H}^* and by the estimate \mathbf{H} .

The alignment error is thresholded to produce the *precision* metric. Following [23] we use two thresholds. The p@5 metric, *i.e.*, the fraction of frames where $e_{\text{AL}} < 5$ px, and the p@15 metric with the e_{AE} threshold set to 15 px.

4.1. POT results

The POT-210 results are summarized in Tab. 2. The proposed WOFTSAM sets a new state-of-the-art performance, almost

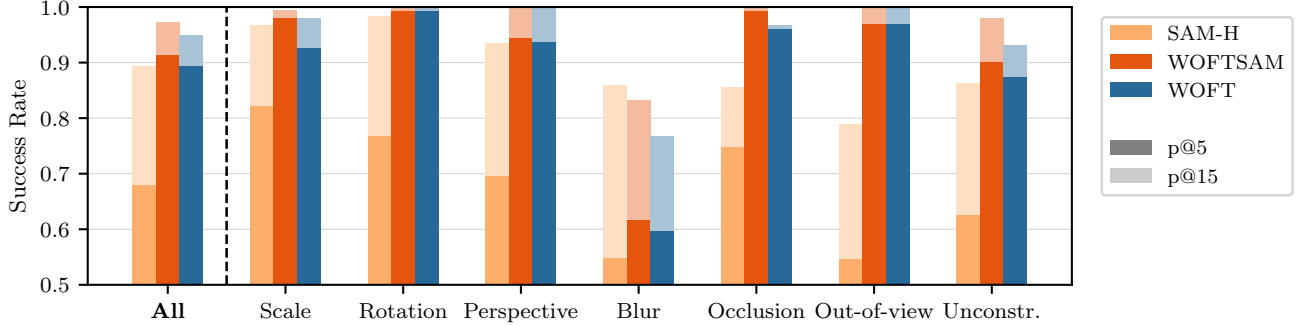


Figure 4. POT-210 [14] overall (*All*) and per-attribute results. Precision measured on 5 px and 15 px alignment error thresholds on the re-annotated GT [23]. Although SAM-H is the least precise of the shown methods, using it as a robust re-detection mechanism in the proposed WOFTSAM outperforms the WOFT [23] baseline, almost halving its failure rate on the 15 px threshold. The improvement is particularly high on the sequences where re-detection is needed — *blur*, *occlusion*, and *unconstrained* — without decreasing performance on the rest of the benchmark.

halving the 15 px alignment error compared to the baseline WOFT. The improvement comes from the proposed re-detection capability as confirmed by the challenging-attribute based analysis shown in Figure 4. Indeed, the most improved attributes are motion *blur* (target impossible to track due to heavy motion blur, followed by re-detection), *occlusion*, and *unconstrained* which contains both blur and occlusions.

Note that the SAM-H re-detection method by itself performs significantly worse ($p@5$ -25.6, $p@15$ -6.4) than the baseline WOFT. The SAM 2 segmentation masks do not provide boundaries precise enough to find the corners to 5 px accuracy. In contrast, the WOFT and WOFTSAM use dense optical-flow-based correspondences from the whole surface of the target, resulting in high precision. The drop in the $p@15$ score is caused mainly by the *occlusion* and *out-of-view* attributes, where often only one or two lines of the target quadrilateral are visible. Since SAM-H estimates the homography pose only from the target boundaries, it fails to provide precise result in such cases. WOFT and WOFTSAM can infer a precise pose from the texture on the visible part of the target. Note that once the whole boundary is visible again SAM-H tends to recover.

The SAM segmentation masks tend to be good even during moderate amount of motion blur, where optical flow and correspondence-based methods cannot work well due to lack of texture, resulting in highest $p@15$ on the *blur* attribute for SAM-H. See Section A in supplementary for success plots and more tracking examples.

4.2. PlanarTrack results

The PlanarTrack results are summarized in Tab. 2. Both SAM-H and WOFTSAM significantly out-perform the previous state-of-the-art WOFT [23] (+18.4 and +7.9 pp on $p@5$, +15.2 and +12.4 pp on $p@15$). Relying on the SAM2 segmentation tracker enables tracking of highly reflective



Figure 5. Typical SAM-H failure cases on the POT-210 [14] dataset. The target is highlighted in *red* on the initial frame. Even when the SAM 2 segmentation works perfectly (not depicted for clarity), occlusions by objects with linear boundaries (b) result in incorrect homographies — SAM-H correctly finds the four corners (not depicted for clarity) of the segmentation mask, but these are no longer the corners of the target object. When the target is partially out-of-view (c), it is easy to distinguish which parts of the mask boundary belong to the object boundary, but there is not enough data to estimate the 8-DoF homography, *e.g.*, one corner and two directions are not enough.

or transparent targets, or even objects with changing appearance, such as TV screens, which was not possible with traditional planar tracking methods. Figure 6 shows that the SAM-H re-detection leads to consistent improvements over the baseline WOFT, especially later in the videos. See Section B in supplementary for results split by challenging attributes and more examples.

WOFTSAM compared to SAM-H. The proposed WOFTSAM achieves lower performance than its re-detection module SAM-H alone on PlanarTrack (-2.8 pp on $p@15$). This is caused by the PlanarTrack containing many sequences where correspondence-based methods are unsuitable due to the properties of the target. These include transparent (a glass pane), highly or fully reflective targets (a mirror), dynamic (a TV screen playing a video) and virtual targets (a hole with planar contour). Optical-flow-based homogra-

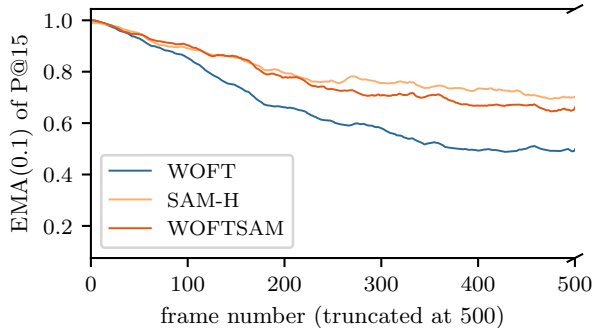


Figure 6. Development of the $p@15$ PlanarTrack_{TST} score in time, smoothed with exponential moving average (EMA) with coefficient 0.1. The x-axis truncated at 500, beyond that the plot becomes noisy due to small number of sequences that long. After about 3.5 seconds of video (\approx frame 100), the SAM-H-based re-detection starts to significantly boost the WOFTSAM performance compared to the baseline WOFT.

phy estimation often does not work well on such targets, or even actively harms the performance. For example, in Seq_00341 (see Section B in supplementary), the target is a mirror that reflects a well textured planar wall on the initial frame. WOFT and WOFTSAM trackers successfully estimate the optical flow tracking the reflected wall, which is indeed a planar target selected in the initial frame, however it is not the *intended* target. In our experiments SAM 2 is sometimes able to segment these kind of targets even with no texture, dynamically changing texture, reflections, *etc.*

On the other hand, there are failure modes for SAM-H that cause WOFTSAM to out-perform it on some sequences. A typical failure case sometimes happens on box-shaped objects in sequences where only one of the box faces is visible in the initial frame. Later in the video, when the camera and/or the object moves and multiple faces become visible, SAM 2 sometimes segments the whole object and not just the face selected on the initial frame (Fig. 10e).

We propose WOFTSAM as a go-to planar tracker achieving overall best performance on POT-210 and PlanarTrack combined, but depending on the type of the tracking scenario, selecting just the SAM-H may be beneficial. We have conducted a per-sequence oracle experiment, where we select the better of WOFTSAM and SAM-H for each sequence of PlanarTrack_{TST}, resulting in 67.1 $p@5$ and 86.9 $p@5$. This is a significant improvement over both WOFTSAM and SAM-H, showing the complementarity of the optical-flow-based and segmentation-based approaches. The complementarity is also demonstrated in Figure 7.

4.3. PlanarTrack GT quality

The annotation quality analysis in the recently accepted journal version of PlanarTrack [12] estimates the mean alignment

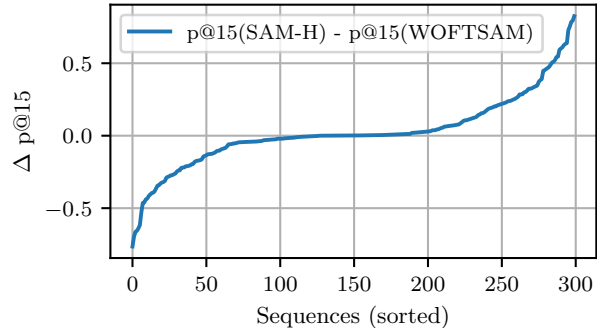


Figure 7. WOFTSAM and SAM-H complementarity on PlanarTrack_{TST} [16]. Per-sequence differences in $p@15$ scores between SAM-H and WOFTSAM show a balance between the sequences where WOFTSAM excels (*bottom left*) and the sequences where SAM-H excels (*top right*). Details in Section 4.2.

error of the original ground truth to be 5.71 px, with more than 10% of annotations exceeding error of 15 px. We have found that inaccurate ground truth accounts for more than half of the $p@5$ score drop between SAM-H and WOFTSAM as described next.

Most planar trackers — including those based on optical flow estimation, like WOFT and the proposed WOFTSAM, keypoint-based trackers, and direct alignment methods — attempt to align the texture of the target in the current frame and in the initial frame. The resulting homography is then applied to the initial control points to get the current frame control point positions. In this scenario, the resulting alignment error of the tracker is affected by the ground truth annotation errors on both the initial and the current frame.

On PlanarTrack, the target is often small on the initial frame and increases in size during the sequence (the target is larger than the init in 59% of frames). This increases the influence of initial frame GT annotations, *i.e.* a N px error in the initial frame results in approximately $s_t \cdot N$ px error in the current frame I_t when the target is $s_t \times$ larger than on I_0 as shown in Figure 8.

We have carefully re-annotated all the PlanarTrack_{TST} initial frames with single pixel or even sub-pixel precision, trying to perfectly align the initial control points with the corners of the target object (see Figure 9, more details in Section C in supplementary). The mean alignment error of the original ground truth on initial frames when compared to the precise re-annotation is only 1.9 px. However, this has significant influence on the evaluation of correspondence based trackers due to the aforementioned scaling as shown in Table 3. In particular, more than half of the PlanarTrack $p@5$ score difference between WOFTSAM and SAM-H is caused by the inaccurate original initial frame annotations.

The effect on the SAM-H results are negligible, because

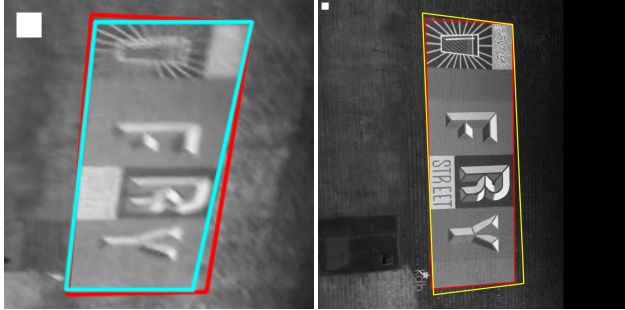


Figure 8. GT annotations (red) on frames I_0 (left) and I_{382} (right) of PlanarTrack Seq_00027. Small pixel error on the low-resolution initial target, compared to precise ground truth (cyan) results in large error when warped (yellow) to a frame with a close-up target view. In particular, the corner pixel errors grew from 6.7, 0.5, 11.1, and 4.1 to 20.1, 1.5, 25.2, and 16.8. The *top-left* corner of each image shows a 20 px \times 20 px white square serving as a scale indicator. Best viewed zoomed in.

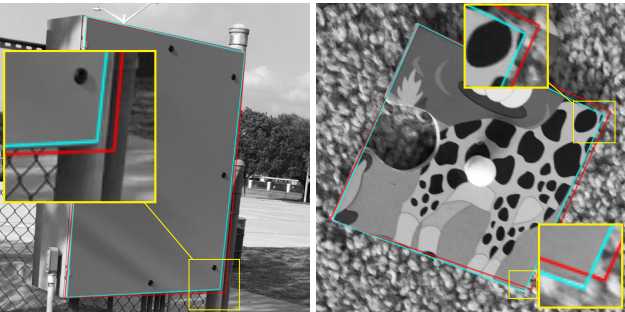


Figure 9. Examples of PlanarTrack_{TST} initial frame precise re-annotation. The original GT (red) goes outside the tracked object, while the new improved GT (cyan) exactly aligns with the target. Best viewed zoomed in, magnified cutouts in yellow. The benchmark scores are affected by both the initial and the current frame GT annotation quality for most planar trackers. Our re-annotation corrects half of the sources of the benchmarking errors. We publish the initial frame re-annotation of the PlanarTrack_{TST} dataset.

SAM-H does not primarily estimate the homography aligning the frames I_0 and I_t . Instead, it directly searches for the corners of the tracked object in I_t and the initial corner points only serve as a rough initialization of the SAM 2 tracker. Note that this also aligns well with what the PlanarTrack annotators did: clicking on the corners of the tracked objects. In essence, SAM-H is able to “guess” the GT even when initialized inaccurately.

5. Limitations and Discussion

The proposed SAM-H and WOFTSAM methods set a new state-of-the-art on the currently most challenging planar tracking benchmark PlanarTrack. However, they have some limitations that should be taken into account when deciding

method	p@5	p@15
WOFT	48.9 (+5.3 pp)	65.9 (+1.1)
WOFTSAM	57.4 (+5.9 pp)	77.6 (+0.4)
SAM-H	62.0 (+0.0 pp)	80.1 (+0.1)

Table 3. PlanarTrack_{TST} evaluation with precisely re-annotated initial frames. Optical flow based methods WOFT [23] and the proposed WOFTSAM greatly benefit from precise initialization. This is because they propagate any errors in initialization to the whole sequence. The effect on SAM-H is negligible, because it estimates the object corner positions directly, only using the initialization for target object selection. Initialization errors are not propagated in this case.

what tracker to use for a particular problem.

While relying on the segmentation tracker for long-term robustness is often beneficial (see Figs. 10a to 10c), the SAM2 fails in some cases. Most notably, it assumes that the target is an “object” with a well defined boundary and it often fails to track arbitrary regions, such as smaller parts of a larger planar surface. A related failure case is that SAM2 sometimes expands to track the whole 3D object and not only its selected planar part, *e.g.*, tracking the whole box, instead of its front face only (Figs. 10d and 10e).

The proposed SAM-H procedure assumes an approximately quadrilateral target shape, which is often the case both in planar tracking benchmarks and in real world, and fails if there are not four stable lines on the target segmentation boundary. Such cases could potentially be detected automatically by initializing the SAM 2 model with a bounding box instead of the segmentation mask and attempting to find the four lines in the first frame output segmentation.

Occlusions (*e.g.* Fig. 10f) pose another issue, unless the underlying segmentation tracker can output amodal segmentation masks. Otherwise occlusions may not be detectable and correctly solvable based solely on the segmentation masks. For example in the POT-210 benchmarks, the majority of partial occlusions are by a piece of paper, meaning that the visible part of the target object forms a perfect quadrilateral even when occluded. Such cases are explained by (incorrect) homographies mapping the whole target to its currently visible part. Additionally, during partial occlusions and out-of-view scenarios it may happen that not all the sides are visible, forcing the SAM-H method to resort to work with less than the full homography 8 degrees of freedom.

In contrast, methods based on dense local correspondences, like WOFT, can estimate the correct homography even during significant occlusions, provided there is enough matchable texture on the visible part. On the other hand, the correspondence-based methods do not work properly when the target lacks enough texture — either as its natural property, or by being blurred by fast motion. They



Figure 10. Examples of SAM 2 [22] output on selected PlanarTrack [16] sequences. The images were cropped around the target from the original full size frames. The initial frames shown on *top* with the ground truth pose in *red*. The *middle row* shows the selected frame with SAM 2 segmentation overlays in *green*. The *bottom row* shows the frame without overlays for better idea of the input data. The first three examples, see Figs. 10a to 10c, are difficult to track with correspondence-based methods, but are segmented well by SAM 2. In Fig. 10d, the segmentation “spills” outside the intended target, but gets corrected in the SAM-H Hough line detection step. Similar situation, but not recoverable by SAM-H is shown in Fig. 10e. Segmentation works well during partial occlusions, but recovering the full pose based only on the mask is not always possible as shown in Fig. 10f. Finally, distractors may cause SAM2 tracking failure (Fig. 10g). Best viewed in color.

also fail completely when the target is transparent (a glass pane: Fig. 1g, a virtual surface of a rectangular hole: Fig. 1d), highly reflective (a mirror: Fig. 1e, a glossy paper, a target behind a glass), or has otherwise changing appearance (a display showing a video: Fig. 1f).

Finally, the recovery after full occlusion, out-of-view motion, or tracking failure is still a major challenge. SAM 2 tends to re-detect well unless there are distractors similar or identical to the target (Fig. 10g). Sometimes such cases cannot be correctly solved without taking into account non-trivial context, *e.g.*, being able to count the third target from left and second from the bottom, which current models cannot reliably do. In scenarios with multiple independently moving distractors, the re-detection may even be impossible. Similarly, the symmetry disambiguation and thus finding the correct pose may be very difficult or impossible with texture-less, low textured, or symmetrically textured targets, without full understanding of the camera ego-motion and the context of the whole scene.

6. Conclusions

The proposed WOFTSAM tracker sets, by a large margin, a new state-of-the-art on both the currently most challenging PlanarTrack [16] benchmark and the POT-210 [14] benchmark. We show that adding the proposed SAM-H geometrical reasoning on top of a general segmentation tracker results

in robust long-term tracking with precise geometrical alignment. The segmentation and the flow-based homography estimation have complementary strengths. Reliably dealing with the cases where they disagree with each other is an interesting future research area as it may be hard to automatically tell which prediction is correct, or that both are wrong. The ability to automatically detect inconsistent pose estimate is also crucial for further research into target re-detection.

Future planar tracking benchmarking efforts should include non-quadrilateral targets and targets that are parts of larger planar surfaces and whose contours are not well defined by image intensity edges. Finally, care must be taken to annotate ground-truth poses accurately and the ground-truth precision should be estimated to set appropriate evaluation metric error thresholds.

We publish the code for SAM-H and WOFTSAM, precise ground-truth re-annotations of the PlanarTrack initial frames, as well as the annotation tools used at <https://github.com/serycjon/WOFTSAM>.

Acknowledgments. This work was supported by the National Recovery Plan project CEDMO 2.0 NPO (MPO 60273/24/21300/21000), the EC Digital Europe Programme project CEDMO 2.0 no. 101158609, and by the Research Center for Informatics project CZ.02.1.01/0.0/0.0/16_019/0000765 funded by OP VVV

References

- [1] Simon Baker and Iain Matthews. Lucas-kanade 20 years on: A unifying framework. *International journal of computer vision*, 56(3):221–255, 2004. 2
- [2] Herbert Bay, Andreas Ess, Tinne Tuytelaars, and Luc Van Gool. Speeded-up robust features (SURF). *Computer vision and image understanding*, 110(3):346–359, 2008. 2
- [3] Selim Benhimane and Ezio Malis. Real-time image-based tracking of planes using efficient second-order minimization. In *2004 IEEE/RSJ International Conference on Intelligent Robots and Systems (IROS)(IEEE Cat. No. 04CH37566)*, pages 943–948. IEEE, 2004. 2
- [4] Selim Benhimane and Ezio Malis. Homography-based 2d visual tracking and servoing. *The International Journal of Robotics Research*, 26(7):661–676, 2007. 1
- [5] Lin Chen, Fan Zhou, Yu Shen, Xiang Tian, Haibin Ling, and Yaowu Chen. Illumination insensitive efficient second-order minimization for planar object tracking. In *2017 IEEE International Conference on Robotics and Automation (ICRA)*, pages 4429–4436. IEEE, 2017. 2
- [6] Lin Chen, Yaowu Chen, Haibin Ling, Xiang Tian, and Yuesong Tian. Learning robust features for planar object tracking. *IEEE Access*, 7:90398–90411, 2019.
- [7] Lin Chen, Haibin Ling, Yu Shen, Fan Zhou, Ping Wang, Xiang Tian, and Yaowu Chen. Robust visual tracking for planar objects using gradient orientation pyramid. *Journal of Electronic Imaging*, 28(1):1–16, 2019. 1, 2, 3
- [8] Richard O Duda and Peter E Hart. Use of the Hough transformation to detect lines and curves in pictures. *Communications of the ACM*, 15(1):11–15, 1972. 3
- [9] Martin A Fischler and Robert C Bolles. Random sample consensus: A paradigm for model fitting with applications to image analysis and automated cartography. *Communications of the ACM*, 24(6):381–395, 1981. 1, 2
- [10] R. I. Hartley and A. Zisserman. *Multiple View Geometry in Computer Vision*. Cambridge University Press, ISBN: 0521540518, 2 edition, 2004. 1
- [11] Paul VC Hough. Method and means for recognizing complex patterns, 1962. 3
- [12] Yifan Jiao, Xinran Liu, Xiaoqiong Liu, Xiaohui Yuan, Heng Fan, and Libo Zhang. Planartrack: A high-quality and challenging benchmark for large-scale planar object tracking. *Computer Vision and Image Understanding*, 262:104553, 2025. 6
- [13] Kunpeng Li, He Liu, and Tao Wang. Centroid-based graph matching networks for planar object tracking. *Machine Vision and Applications*, 34(2):31, 2023. 2, 4
- [14] Pengpeng Liang, Yifan Wu, Hu Lu, Liming Wang, Chunyuan Liao, and Haibin Ling. Planar object tracking in the wild: A benchmark. In *2018 IEEE International Conference on Robotics and Automation (ICRA)*, pages 651–658. IEEE, 2018. 1, 2, 3, 4, 5, 8
- [15] Pengpeng Liang, Haoxuanye Ji, Yifan Wu, Yumei Chai, Liming Wang, Chunyuan Liao, and Haibin Ling. Planar object tracking benchmark in the wild. *Neurocomputing*, 454:254–267, 24 September 2021, 2021. 1
- [16] Xinran Liu, Xiaoqiong Liu, Ziruo Yi, Xin Zhou, Thanh Le, Libo Zhang, Yan Huang, Qing Yang, and Heng Fan. PlanarTrack: A large-scale challenging benchmark for planar object tracking. In *Proceedings of the IEEE/CVF International Conference on Computer Vision (ICCV)*, pages 20449–20458, 2023. 1, 2, 3, 4, 6, 8, 5
- [17] Yuan Liu, Zehong Shen, Zhixuan Lin, Sida Peng, Hujun Bao, and Xiaowei Zhou. GIFT: Learning transformation-invariant dense visual descriptors via group cnns. *Advances in Neural Information Processing Systems*, 32, 2019. 2
- [18] David G Lowe. Distinctive image features from scale-invariant keypoints. *International journal of computer vision*, 60(2):91–110, 2004. 1, 2, 4
- [19] Bruce D Lucas and Takeo Kanade. An iterative image registration technique with an application to stereo vision. In *Proceedings of the 7th International Joint Conference on Artificial Intelligence-Volume 2*, pages 674–679, 1981. 1, 2
- [20] Maxime Oquab, Timothée Darcet, Théo Moutakanni, Huy Vo, Marc Szafraniec, Vasil Khalidov, Pierre Fernandez, Daniel Haziza, Francisco Massa, Alaaeldin El-Nouby, et al. DINOv2: Learning robust visual features without supervision. *arXiv preprint arXiv:2304.07193*, 2023. 3, 4
- [21] Rémi Pautrat, Viktor Larsson, Martin R Oswald, and Marc Pollefeys. Online invariance selection for local feature descriptors. In *European Conference on Computer Vision*, pages 707–724. Springer, 2020. 2, 4
- [22] Nikhila Ravi, Valentin Gabeur, Yuan-Ting Hu, Ronghang Hu, Chaitanya Ryali, Tengyu Ma, Haitham Khedr, Roman Rädle, Chloe Rolland, Laura Gustafson, Eric Mintun, Junting Pan, Kalyan Vasudev Alwala, Nicolas Carion, Chao-Yuan Wu, Ross Girshick, Piotr Dollár, and Christoph Feichtenhofer. SAM 2: Segment anything in images and videos. *arXiv preprint*, 2024. 1, 2, 3, 4, 8
- [23] Jonáš Šerých and Jiří Matas. Planar object tracking via weighted optical flow. In *Proceedings of the IEEE/CVF Winter Conference on Applications of Computer Vision*, pages 1593–1602, 2023. 1, 2, 3, 4, 5, 7
- [24] Zachary Teed and Jia Deng. RAFT: Recurrent all-pairs field transforms for optical flow. In *European Conference on Computer Vision*, pages 402–419. Springer, 2020. 1, 4
- [25] Jovana Videnovic, Alan Lukezic, and Matej Kristan. A distractor-aware memory for visual object tracking with sam2. In *Proceedings of the Computer Vision and Pattern Recognition Conference*, pages 24255–24264, 2025. 2, 4
- [26] Tao Wang and Haibin Ling. Gracker: A graph-based planar object tracker. *IEEE transactions on pattern analysis and machine intelligence*, 40(6):1494–1501, 2017. 1, 2
- [27] Xinrui Zhan, Yueran Liu, Jianke Zhu, and Yang Li. Homography decomposition networks for planar object tracking. In *Proceedings of the AAAI Conference on Artificial Intelligence*, pages 3234–3242, 2022. 2, 4
- [28] Haoxian Zhang and Yonggen Ling. HVC-Net: Unifying homography, visibility, and confidence learning for planar object tracking. In *Computer Vision and Pattern Recognition (CVPR)*, 2022. 1, 2, 4

Accurate Planar Tracking With Robust Re-Detection

Supplementary Material

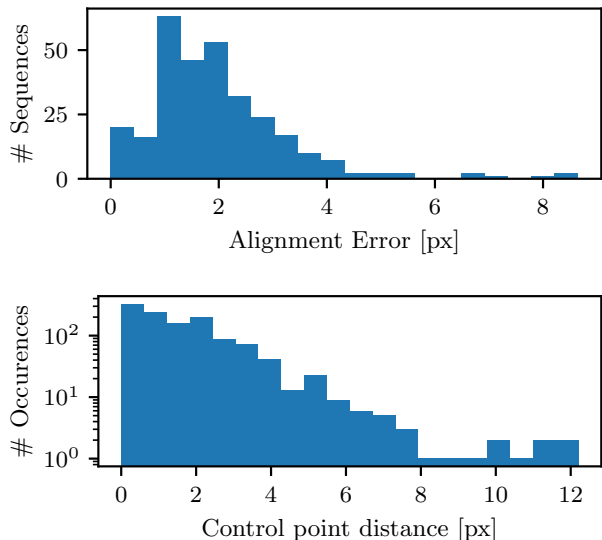


Figure S1. Error histograms of the original PlanarTrack_{TST} [16] initial frame annotations compared to our re-annotation. *Top*: alignment error e_{AL} , capturing the annotation difference over all the four control points (RMSE). *Bottom*: euclidean distance of individual control point positions, with y-axis scaled logarithmically.

A. Detailed POT-210 Results

We provide the commonly reported alignment error success plots in Figure S2. WOFTSAM consistently out-performs the baseline WOFT [23]. At the 15 px alignment error threshold, the failure rate is almost halved. The improvement comes mainly from the *blur*, *occlusion*, and *unconstrained* sequences, where the re-detection ability is most needed. Robust re-detection also helps in some of the *scale* sequences, where the baseline WOFT fails to keep track of a small (zoomed out) object. Some examples of the WOFTSAM, SAM-H and WOFT outputs are shown in Figure S3.

B. Detailed PlanarTrack Results

Similar to POT-210, we show the success rate curves for the PlanarTrack [16] dataset in Figure S5. The plots show the proposed WOFTSAM to be consistently better than WOFT [23] on all error thresholds.

Note that in contrast to POT-210 (where each video is of one type, *e.g.* *occlusion*, or *scale*), each video is assigned multiple challenging attributes in PlanarTrack. For example, 271 of the 300 sequences have four or more attributes assigned (out of the total of eight), and 114 sequences have six or more attributes. Consequently, the per-attribute results

are not easily interpretable. Most common combinations of attributes are shown in Figure S6. In general, the PlanarTrack sequences would be categorized as *unconstrained* in the POT-210 terminology.

Examples of sequences, where SAM-H and WOFTSAM significantly differ are shown in Figure S4.

C. Re-Annotation Details

The annotation tool is controlled by keyboard, allowing the annotator to select a control point to move and moving it up, down, left, or right in increments of N px. The movement step is set to $N = 1$ by default, but can be repeatedly multiplied or divided by 2 to correct larger errors and fine-tune precisely. Apart for a zoomed-in view of the initial frame and the control-point-defined quadrilateral, the annotation tool also shows a later frame for reference. By default, the frame with the largest target object area is shown, but the video can be stepped in both directions to show a different reference frame. This is to ensure that we adhere precisely to what the original annotators were annotating. Moreover, a third view shows image intensity alignment between the current initial frame annotation and the selected reference frame GT. This way, the annotator can find a precisely annotated reference frame and manually align the initial frame with it, to achieve sub-pixel precision. Examples of the resulting re-annotation quality are shown in Figure S7, in addition to Figure 9 in the paper.

Error statistics of the original GT annotations compared to our re-annotation are shown in Figure S1. Note how relatively small alignment error of the first frame annotation significantly affects the evaluation results (Table 3 in the paper). The annotation tool is publicly available together with the WOFTSAM and SAM-H code at <https://github.com/serycjon/WOFTSAM>.

D. Failure Detection Threshold Sensitivity

For failure detection, we used the 20% inlier threshold from WOFT without tuning it. In Table S1 we provide results with different values of the inlier threshold hyper-parameter, showing that WOFTSAM is stable over wide range of thresholds.

E. WOFTSAM efficiency

We evaluated the efficiency on the PlanarTrack_{TST} dataset. Overall, including loading the 1280×720 images from disk, the proposed WOFTSAM runs at 422 ms/frame (2.4 FPS), using a NVIDIA RTX A5000 GPU, requiring 4.5GB of GPU

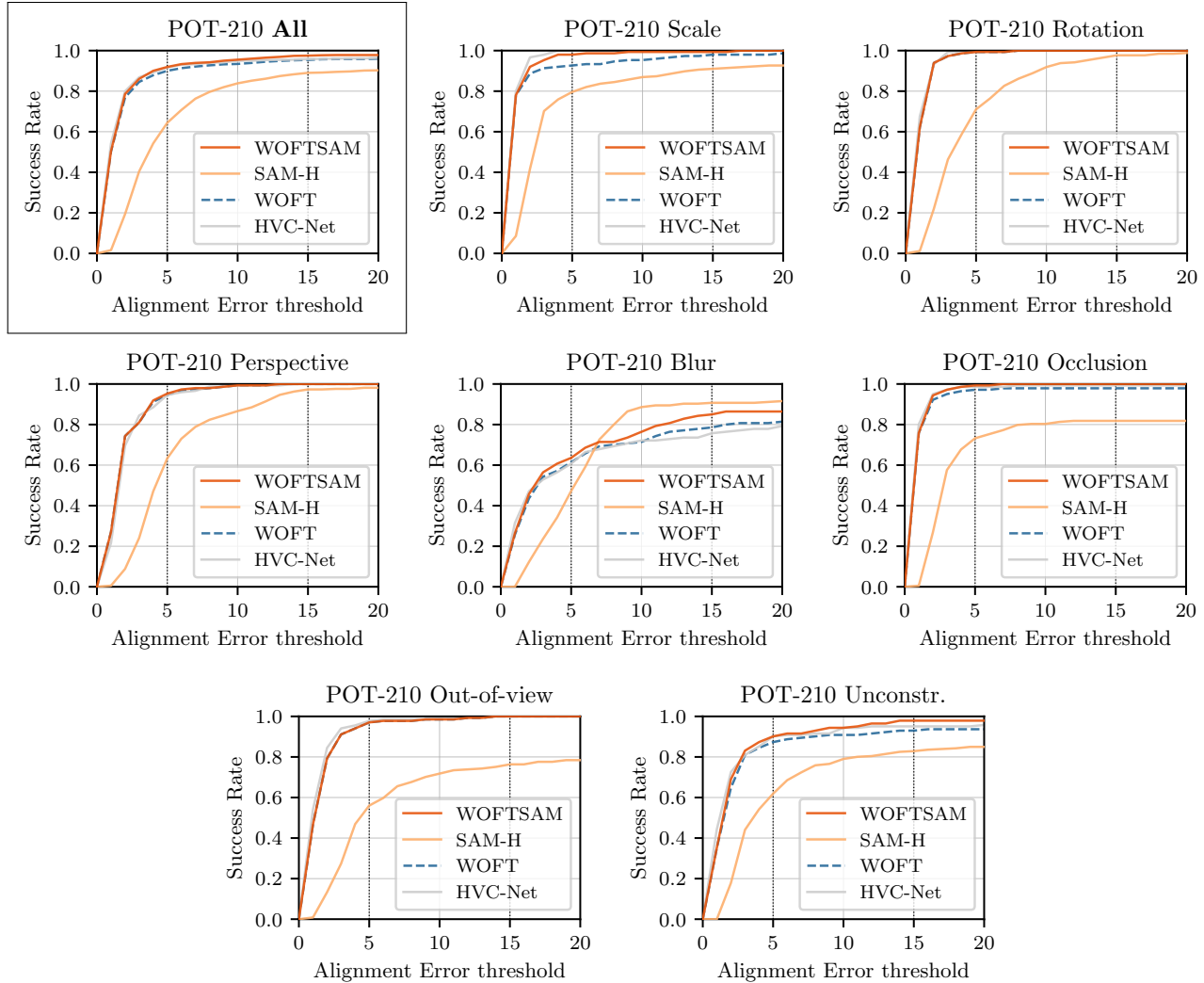


Figure S2. Alignment Error success plots on POT-210 [14], with precise GT re-annotation from [23]. The results are shown on the whole dataset (**All**) and also split by the POT-210 challenge types. Thanks to the proposed SAM-H-based re-detection scheme, WOFTSAM performs better than the WOFT baseline. The $p@5$ and $p@15$ metric thresholds highlighted.

RAM (and Intel(R) Xeon(R) Gold 6326 CPU). On the same device, WOFT runs at a similar speed of 2.7 FPS.

Here we provide a detailed analysis of the runtime of the most heavy parts of the computation. The SAM2 segmentation takes only 42ms per frame (using the hiera tiny SAM2.1 model), which could be further reduced or even removed by computing the segmentation in parallel with the first pre-warped + Weighted-Flow-Homography (part 1 in Figure 3 in the paper). The DINOv2-based symmetry resolution takes 102ms on average, but is only used in around 5% of frames, resulting in amortized 5ms runtime. A single RAFT optical flow computation takes 170ms on average. The Hough line detection and post-processing takes 132ms on average, which would be significantly improved by rewriting from Python to e.g. C/C++. The most computationally costly part

is the optical flow, just like in WOFT. While the WOFTSAM doesn't currently run real-time, it is usable for interactive applications like tracking in movie post-production.

F. Hough Transform Details

This section describes the implementation details of the Hough transform for line detection. First, we discard all mask contours shorter than 20 px (SAM noise) and normalize the rest to have zero mean, moving the center of the target into origin. Then we do the Hough voting followed by least squares refinement. The Hough accumulator represents the lines with normal angle quantized to 359 values, *i.e.*, 1° step, and 100 distances from origin, spanning from 0 to maximum distance of a contour point. We traverse the contours one-by-



Figure S3. POT-210 [14] examples, where outputs of WOFTSAM (dark orange) significantly differ from the outputs of SAM-H (light orange) or WOFT (blue). SAM 2 mask shown as a green overlay, frames are cropped around the object.

Top: SAM-H homography incorrect due to occlusion with a linear boundary. WOFT and WOFTSAM outputs overlap. Frames $I_0, I_{341}, I_{343}, I_{345}, I_{347}$ of $V30_5$.

Bottom: WOFT switches to tracking an incorrect target during occlusion (middle image). SAM-H stays on the correct object, although with an incorrect homography during the occlusion. WOFTSAM stays on the correct target thanks to the robust re-detection (last image). WOFT and WOFTSAM outputs overlap on the first two images. Frames $I_0, I_{65}, I_{77}, I_{137}, I_{176}$ of $V10_5$.



Figure S4. PlanarTrack [16] examples, where the outputs of the flow-based WOFTSAM (dark orange) significantly differ from the outputs of segmentation-based SAM-H (light orange). SAM 2 mask shown as a green overlay, frames are cropped around the object.

Top: While SAM and consequently SAM-H tracks the mirror surface as annotated in the dataset, WOFTSAM tracks a different planar surface (the doors and part of the adjacent wall) reflected in the mirror. Frames $I_0, I_{20}, I_{40}, I_{60}, I_{80}$ of Seq_00341.

Bottom: Two failure modes of SAM-H. (i) SAM 2 segments correctly, but the homography estimation is incorrect due to an occlusion (middle image). (ii) SAM 2 “spills” beyond the prompted surface (last two images). Frames $I_0, I_{20}, I_{90}, I_{175}, I_{195}$ of Seq_00926.

one. For each contour point x_i , we compute the contour direction as the angle α_i between x_{i-4}, x_{i+4} (indexes modulo contour length). Each point casts multiple votes for lines going through it. In particular we consider lines differing from

the angle α_i by $\Delta\alpha \in \{-10^\circ, -8^\circ, \dots, 0^\circ, \dots, +10^\circ\}$ (11 votes). We ensure that distances are non-negative by rotating 180° when needed. The votes are weighted by $w = 1 - \frac{|\Delta\alpha|}{20}$,

inlier threshold	POT-210		PT _{TST}	
	p@5	p@15	p@5	p@15
10%	91.9	97.3	50.2	75.0
20%	91.9	97.5	51.5	77.2
30%	91.6	97.7	52.0	77.6

Table S1. WOFTSAM sensitivity to the failure detection threshold hyper-parameter. The results are stable over a wide range of thresholds. In PT_{TST}, the results slightly improve when increasing the threshold, consistently with the WOFTSAM vs SAM-H results as discussed in the paper. Even with the worst-performing 10% threshold, WOFTSAM out-performs the second-best WOFT by a large margin (+10.2pp). POT-210 results with the improved annotations from the WOFT paper, PlanarTrack_{TST} (PT_{TST}) as in Table 2 in the paper.

assigning full weight 1 to the original α_i , half the weight 0.5 to the extremes $\alpha_i \pm 10^\circ$, and linearly ramping in between.

Next we find peaks in the accumulator. We repeat the accumulator 3 times side by side (unwrapping the periodic angle axis), and perform a Gaussian filtering with $\sigma = 4$. To find peaks in the resulting smoothed accumulator, we use `find_peaks` from SciPy, with minimal peak distance of 10. After undoing the accumulator unwrap, *i.e.*, discarding the peaks from its first and its last repetition, only keeping the peaks in the middle, we take the top $K = 4$ ones, sort them by the angle and convert back to line equations in the original image coordinates.

This procedure is followed by a refinement step. The contours are traversed once again, computing the direction α_i between x_{i-4}, x_{i+4} as before. The contour point x_i is assigned to the closest one of the four Hough-detected lines l_j , if it is close enough, $d(x_i, l_j) \leq 15$ px and the direction α_i is less than 15° from the Hough line direction β_j . After collecting these support points $S_j = \{x_i \mid i = \arg \min_i \text{dist}(x_i, l_j); d(x_i, l_j) \leq 15 \text{ px}; d(\alpha_i, \beta_j) \leq 15^\circ\}$ for each line, the lines get re-computed by a least-squares fit through their supporting points S_j . The code is available at <https://github.com/serycjon/WOFTSAM>.

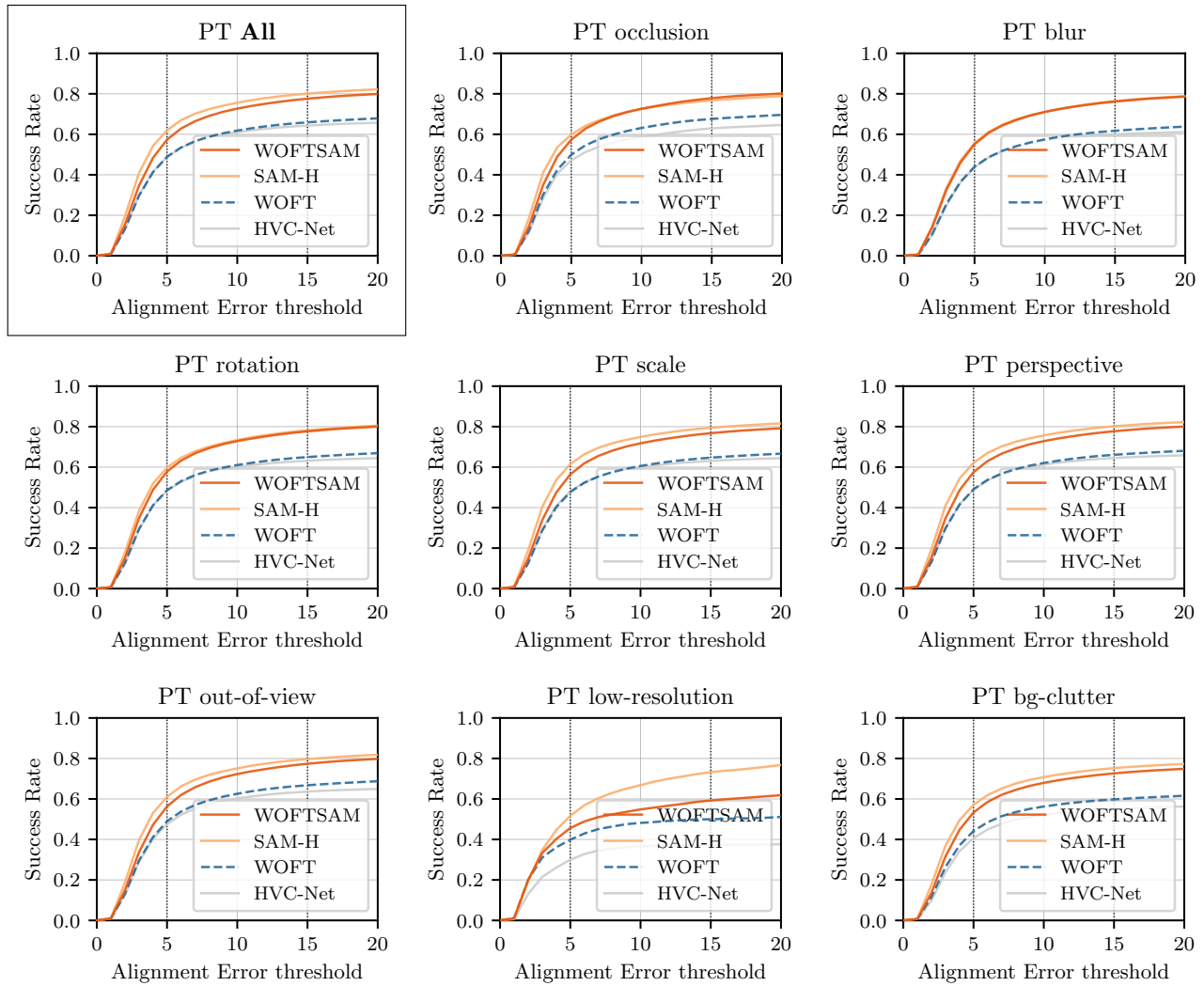


Figure S5. Alignment Error success plots on PlanarTrack_{TST} [16], with our precise GT re-annotation of the initial frame. The results are shown on the whole dataset (**All**) and also split by the PlanarTrack challenging attributes. Thanks to the proposed SAM-H-based re-detection scheme, WOFTSAM performs better than the WOFT baseline. The SAM-H alone performs the best, as discussed in Section 4.2 in the paper. The p@5 and p@15 metric thresholds highlighted. Note that each video may have multiple attributes, unlike in POT-210.

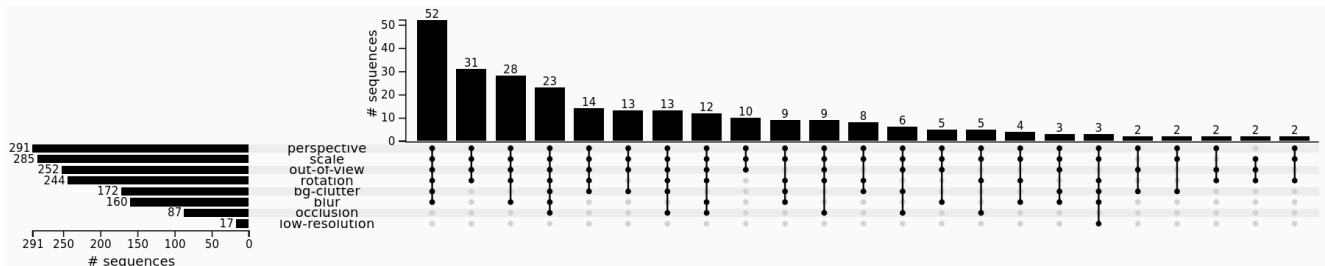


Figure S6. Most frequent combinations of challenging attributes in the PlanarTrack_{TST} [16] dataset. Challenging attributes in rows, their combinations in columns. For example, 28 sequences have the following combination of attributes: *perspective, scale, out-of-view, rotation, blur*. Visualized using <https://upset.js.org> based on *UpSet: visualization of intersecting sets* by Lex et al.



Figure S7. Examples of our PlanarTrack_{TST} [16] re-annotation on the initial frames. The original GT (*red*) does not copy the object boundaries precisely, while the new improved GT (*cyan*) aligns with the target.